Modelling the disc edge vortices for propellers of multirotor eVTOL in forward flight

Furkat Yunus[1] Assistant Professor

Gianluca Romani[2] Software Engineering Manager

Damiano Casalino[2] R&D Technology Director

Marilena Pavel[1] Associate Professor

Mirjam Snellen[1] Full Professor

[1] Control and Operations Department, Faculty of Aerospace Engineering, Delft University of Technology, Delft, The Netherlands

[2] SIMULIA Fluids R&D, Dassault Systemes Deutschland GmbH, Stuttgart, Germany

ABSTRACT

This paper presents a computational method that couples the Peters–He finite-state dynamic inflow model with both an analytical and a prescribed wake model to predict the lateral and axial positions of roll-up and tip vortices, respectively, during forward flight. The analytical wake model, originally developed for helicopter rotors, is extended to predict the position and geometry of disc edge vortices in flight conditions with advance ratios above 0.15. The prescribed wake model is based on the Beddoes formulation. Validation against high-fidelity CFD simulations shows good agreement with the proposed approach. The results suggest that this method provides a reliable and computationally efficient alternative to mid-fidelity techniques such as free-vortex wake models and can be readily integrated with dynamic inflow models to simulate rotor–rotor aerodynamic interactions.

NOTATION

*

Symbols

α_d disk angle of attack, rad

N_b number of blades

m number of harmonics

n highest power in the Legendre polynomials

R Rotor radius, m

Γ circulation, m^2/s

x, y, z Cartesian coordinates, m

μ advance ratio;$\mu = V\cos\alpha_d/V_t$

μ_∞ advance ratio;$\mu_\infty = V/V_t$

V free stream velocity, m/s

V_t tip velocity; $V_t = \Omega R$, m/s

ζ, η Cartesian coordinates, meter

r, φ polar coordinates, m, rad

Z length of the vortex sheet that has rolled up into a disc edge during time t, m

κ constant in circulation distribution, $\mathrm{m}^{3/2}/\mathrm{s}$

ψ azimuth angle, rad

ψ_b blade azimuth angle, deg

$\bar{\psi}_w$ wake age, deg

$\{X\}$ inflow state vector

$\{\dot{X}\}$ azimuthal derivative of inflow state vector

$[M]$ apparent mass matrix

$[L]$ influence matrix

$\{\tau\}$ inflow forcing function

v_d downward velocity at the trailing edge,m/s

$[e]$ distance behind the rotor where a disc edge vortex is fully formed, m

t time, s

v_i rotor or wake induced velocity, m/s

r_v normalized radial release point with respect to the rotor radius

Ω rotational speed, rad/s

λ_i induced inflow ratio; $\lambda_i = v_i/\Omega R$

INTRODUCTION

In recent years, advances in electric propulsion have opened the door to a new era of air mobility, driven by electric vertical takeoff and landing (eVTOL) technology. In this new "aviation golden age", the vehicles are often powered by multiple rotors to realize vertical takeoff and landing capability and maneuverability. With the growing number of eVTOL developments, efforts need to be undertaken in predicting their aerodynamic behaviour in different flight conditions. The wake of a propeller is characterized by multiple structures, including the blade-tip vortex, the rotor downwash, the blade shear layers, and the surrounding external flow (Ref. Komerath et al., 2011). During forward flight, tip-vortices generated by a rotor roll into two counter-rotating disc-edge vortices, similar to the tip vortices formed behind a fixed-wing aircraft. In helicopters, these vortices are large and powerful, often affecting the tail rotor during direct interaction. This interaction can have a significant impact on the helicopter ability to maintain control and stability (Ref. Wang et al., 2021).

A similar wake roll-up process (see Fig. 2) occurs for the propellers of multirotor systems. However, unlike helicopters, multirotor systems feature closely spaced rotors, and the disc edge vortices generated by these rotors significantly affect the performance of downstream rotors (Ref. Misiorowski et al., 2019). These vortices impact not only the stability and control of the system as a whole, but also its overall aerodynamic performance and noise generation. Accurate prediction of spatial position and geometries of rotor tip and rolled-up edge vortices is essential for predicting rotor-rotor blade-wake-interaction (BWI) and rotor-airframe interactions, as well as the associated noise generation in forward flight (Ref. Luo et al., 2015), which is crucial for optimizing both multirotor aircraft performance and noise reduction.

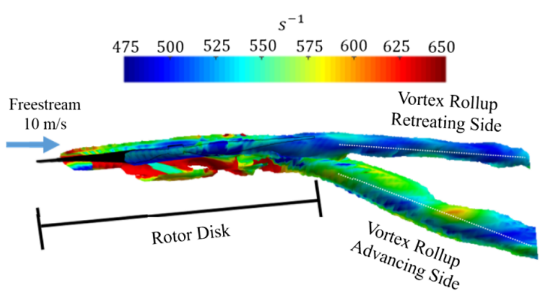

Figure 1: Rotor wake from an isolated rotor in forward flight (Ref. Misiorowski et al., 2019).

The primary objective of this paper is to present a computational approach for predicting the spatial position and geometry of rotor tip vortices and roll-up disc-edge vortices in propellers typically used in multirotor eVTOL aircraft. The method combines the Peters–He finite-state dynamic inflow model, which provides the necessary aerodynamic performance data, with vortex trajectory prediction models. Tip vortex trajectories are estimated using the Beddoes prescribed wake model, while disc-edge vortex locations are predicted by extending an analytical model originally developed for helicopter rotors operating at advance ratios above 0.15 (Ref. Roos, 1996). This extended model is adapted for eVTOL propellers, which operate at significantly lower Reynolds numbers—approximately one order of magnitude lower than conventional helicopter rotors (Ref. Casalino et al., 2021).

The core contribution of this work lies in coupling the Peters–He finite-state dynamic inflow model with both analytical and prescribed wake models and validating the resulting predictions against high-fidelity CFD simulations in forward flight. Rotor–airframe interactions and noise generation, which are important in multirotor systems, are not addressed here; these aspects are covered in a companion paper by the authors (Ref. Yunus et al., 2025).

It is also worth noting that Luo et al. (Ref. Luo et al., 2015) proposed an analytical model for disc-edge vortices in quadrotors. However, their approach did not capture key physical effects, such as the differences in vortex roll-up between advancing and retreating blades, nor did it account for the lateral and axial variation in vortex positions or the distribution of circulation—factors. Instead, both these features are explicitly addressed in the present work.

OVERVIEW OF THE COMPUTATIONAL APPROACH

Aerodynamic model

The aerodynamic loading on the rotor disk is computed by coupling the Peters–He finite-state dynamic inflow model (Ref. Peters and He, 1995) with blade element momentum theory (BEMT). A comprehensive overview of the underlying theory and the development of the finite-state inflow model is provided in (Refs. Peters and He, 1995,Moriarty and Hansen, 2005,Li, 2020).

The theoretical foundation of the Peters–He model lies in the actuator disk solution to the three-dimensional potential flow equations (Ref. Kinner, 1937). In this formulation, the normal component of the induced velocity on the rotor disk is represented as a double-infinite series expansion, comprising azimuthal Fourier harmonics and radial Legendre functions. By truncating this infinite series to a finite number of terms, a finite set of inflow states is obtained. These states describe the induced velocity field over the rotor disk and are governed by the following system of ordinary differential equations (ODEs):

$$\left[M\right]\left\{\dot{X}\right\}+\left[L\right]^{-1}\left\{X\right\}=\left\{\tau\right\} \tag{1}$$

where $\left[M\right]$ is the apparent mass (or time) matrix, $\left\{X\right\}$ is the inflow states vector, and $\left\{\dot{X}\right\}$ is its time derivative. The matrix $\left[L\right]$ is the influence matrix, while the term $\left\{\tau\right\}$ on the right-hand side represents the inflow forcing function, which depends on the aerodynamic loads and is typically obtained using blade element theory. Physically, Eq.(1) describes how the rotor loading τ is influenced by a combination of unsteady inflow dynamics, governed by the time matrix $\left[M\right]$, and steady inflow effects, governed by the influence matrix $\left[L\right]$.

The induced velocity on the rotor disk is truncated using a finite number of Fourier harmonics in the azimuthal direction and Legendre functions in the radial direction, where the latter are defined by Legendre polynomials. This formulation results in what is referred to as an m-by-n dynamic inflow model. The parameters m and n are defined by the user and must be selected to balance model accuracy with computational efficiency, particularly in design applications. In most practical implementations, the parameter m is related to the number of blades. For example, in (Ref. Usov et al., 2022), m was set equal to the number of blades N_b, which was found to be sufficient for steady-state predictions, while n (denoted as p in their formulation) was set to 4 to ensure convergence of the aerodynamic loads. In contrast, (Ref. Ho and Yeo, 2021) sets both m and n to $3N_b$ to balance accuracy and computational efficiency. Following this approach, the present study adopts $m = 3N_b$ and $n = 3N_b$. Eq. 1 is integrated in dimensionless time using a fourth-order Runge–Kutta (RK4) scheme. Unless otherwise stated, all calculations in this paper use 90 azimuthal steps per revolution.

Analytical wake model

The analytical formulation proposed by Roos (Ref. Roos, 1996) was originally developed based on the classical fixed-wing theory by Kaden (Ref. Kaden, 1931), which models the rotor wake as a wing wake rolling up into two edge vortices at the periphery of the rotor disc. This time-averaged analytical model determines the position, geometry, and strength of these vortices. Only rotor geometry, rotor speed, tip speed, thrust coefficient, and air density are required as input parameters. However, when predictions based on these parameters were applied in this work, unexpected results are observed, particularly in estimating the center of gravity of vortex cores on both sides of the rotor disc and the wake asymptotes beyond which the wake is assumed to be fully rolled up. Consequently, several modifications are introduced to extend the model for propellers used in multirotor systems. A brief overview of the analytical model and the modifications is provided below; for further details, the reader is referred to the original work (Ref. Roos, 1996).

Kaden demonstrated that the lateral coordinates of the vortex centers (see Fig. 2a) as they develop are given by:

$$\begin{aligned} \zeta_c &= 0.57Z, \\ \eta_c &= 0.88Z, \end{aligned} \tag{2}$$

The quantity Z represents the length of the vortex sheet that has rolled up into discrete vortices by time t, measured from the onset of the rolling-up process (see Fig. 2a). For both the advancing and retreating sides of the rotor disk, it is defined as:

$$\begin{aligned} \bar{Z}_{\text{adv}} &= R^{-1/3}\left(\frac{9}{2\pi^2}\kappa_{\text{adv}}\frac{\bar{x}_c}{V}\right)^{2/3}, \\ \bar{Z}_{\text{retr}} &= R^{-1/3}\left(\frac{9}{2\pi^2}\kappa_{\text{retr}}\frac{\bar{x}_c}{V}\right)^{2/3}. \end{aligned} \tag{3}$$

Here, κ is a parameter that arises in the derivation of the circulation distribution over the rotor disk, which is given as:

$$\begin{aligned} \kappa_{\text{adv}} &= \frac{\sqrt{2}}{2\pi\mu\sqrt{R}}\Gamma_0\left(1-\frac{3}{2}\mu\right), \\ \kappa_{\text{retr}} &= \frac{\sqrt{2}}{2\pi\mu\sqrt{R}}\Gamma_0\left(1+\frac{3}{2}\mu\right), \end{aligned} \tag{4}$$

where Γ_0 is the constant term in the blade circulation, defined by the expression $\Gamma = \Gamma_0 + \Gamma_1 \sin\psi$. This circulation model assumes that the only significant variation arises from the azimuthal dependence of the blade circulation $\Gamma(\psi)$, based on the observation that the rapid formation of blade tip vortices gives the appearance of trailing from a blade with spanwise-constant circulation. It is further assumed that the rotor is in momentum equilibrium and generates sufficient thrust to counteract the helicopter weight and drag. It should be noted that, in the present work, the blade circulation Γ, along with Γ_0 and Γ_1, is directly obtained from the Peters–He finite-state dynamic inflow model. In contrast, in the work of Roos (Ref. Roos, 1996), these quantities were estimated based on the helicopter weight and flight condition. The lateral positions of the disc edge vortices are then given by:

$$\begin{aligned} \bar{y}_{c,\text{adv}} &= 0.57\bar{Z}_{\text{adv}}, \\ \bar{y}_{c,\text{retr}} &= 0.88\bar{Z}_{\text{retr}}. \end{aligned} \tag{5}$$

Equation (5) provides an acceptable approximation of the vortex lateral positions close to the rotor. However, it does not capture the known asymptotic positions far downstream. The far-field lateral positions of the vortices are determined by the principle that a fully formed vortex coincides with the center of gravity of the portion of the vortex sheet from which it originates. To find the asymptotic vortex locations, it is assumed that the lateral position of the center of gravity remains invariant throughout the roll-up process (Ref. Spreiter and Sacks, 1951). Under this assumption, it can be determined by considering the center of gravity position of a flat vortex sheet:

$$\bar{y}_{\text{cg}} = \frac{y_{\text{cg}}}{R} = \frac{1}{R}\frac{\int \frac{\partial\Gamma}{\partial y} y\,dy}{\int \frac{\partial\Gamma}{\partial y}dy} = \frac{\int \frac{\partial\Gamma}{\partial\bar{y}}\bar{y}\,\mathrm{d}\bar{y}}{\int \frac{\partial\Gamma}{\partial\bar{y}}\mathrm{d}\bar{y}} \tag{6}$$

The integration limits are set by the portions of the vortex sheet that roll up into each disc edge vortex: $-1 \leq \bar{y} < \bar{y}(\Gamma = \Gamma_{\max})$ on the retreating side, and $\bar{y}(\Gamma = \Gamma_{\max}) \leq \bar{y} \leq 1$ on the advancing side. On the advancing side, the intersection point at which Kaden's solution meets the asymptote is determined by the condition $\bar{y}_{\text{cg,adv}} = 1 - 0.57, \bar{Z}_{\text{adv}}$. The corresponding intersection locations on the advancing and retreating sides

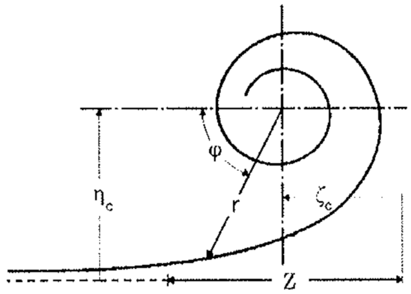

(a) Definition of ζ and η,

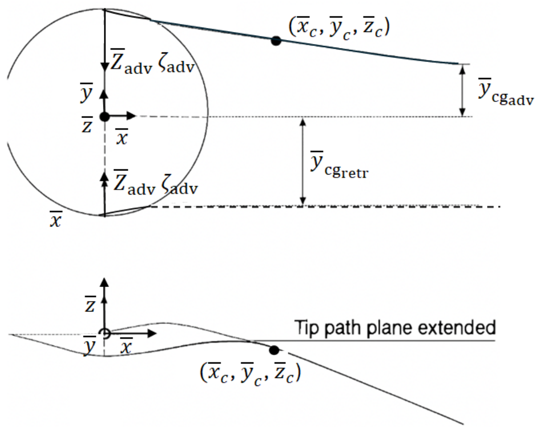

(b) Definition of edge vortex coordinates.

Figure 2: (a) Geometrical definition of lateral coordinates of the centers of the developing vortices. (b) Lateral locations of center of gravity on both advancing and retreating sides.

are denoted by $\bar{s}_{\text{adv}}$ and $\bar{s}_{\text{retr}}$, respectively. By substituting Eq. 3, the following expression is obtained:

$$\begin{aligned}\bar{s}_{\text{adv}} &= \frac{2}{9}\pi^2 R^{1/2}\left(\frac{1}{0.57}\left(1-\bar{y}_{\text{cg,adv}}\right)\right)^{3/2}\frac{V}{\kappa_{\text{adv}}},\\ \bar{s}_{\text{retr}} &= \frac{2}{9}\pi^2 R^{1/2}\left(\frac{1}{0.57}\left(1+\bar{y}_{\text{cg,adv}}\right)\right)^{3/2}\frac{V}{\kappa_{\text{retr}}},\end{aligned} \tag{7}$$

Beyond these points, the lateral positions of the disc edge vortices remain constant and are given by:

$$\begin{aligned}\bar{y}_{\text{c,adv}} &= \bar{y}_{\text{cg,adv}} \quad \text{for} \quad \bar{x} \geq \bar{s}_{\text{adv}},\\ \bar{y}_{\text{c,retr}} &= \bar{y}_{\text{cg,retr}} \quad \text{for} \quad \bar{x} \geq \bar{s}_{\text{retr}}.\end{aligned} \tag{8}$$

Closer to the rotor, the approximate axial positions of the disc edge vortices are given by:

$$\begin{aligned}\bar{z}_{\text{c,adv}} &= 0.88\bar{Z}_{\text{adv}} - \frac{v_{\text{d,adv}}}{V}\bar{x} \quad \text{for} \quad \bar{x} \leq \bar{e}_{\text{adv}},\\ \bar{z}_{\text{c,retr}} &= 0.88\bar{Z}_{\text{retr}} - \frac{v_{\text{d,retr}}}{V}\bar{x} \quad \text{for} \quad \bar{x} \leq \bar{e}_{\text{retr}},\end{aligned} \tag{9}$$

In the far field, after the vortices have fully rolled up, their axial positions are described by:

$$\begin{aligned}\bar{z}_{\text{c,adv}} &= \bar{z}_{\text{c,adv}}(\bar{x}=\bar{e}_{\text{adv}}) - \frac{v_{\text{d},\infty}}{V}(\bar{x}=\bar{e}_{\text{adv}}) \quad \text{for} \quad \bar{x} > \bar{e}_{\text{adv}},\\ \bar{z}_{\text{c,retr}} &= \bar{z}_{\text{c,retr}}(\bar{x}=\bar{e}_{\text{retr}}) - \frac{v_{\text{d},\infty}}{V}(\bar{x}=\bar{e}_{\text{retr}}) \quad \text{for} \quad \bar{x} > \bar{e}_{\text{retr}},\end{aligned} \tag{10}$$

Here, $v_d = v_i + V\alpha_d$ denotes the downward velocity at the trailing edge, where v_i is the induced velocity at the rotor tip. This relation is used to determine the downward velocities of the vortices on both the advancing and retreating sides of the rotor. In this work, v_d is taken equal to v_i which is obtained directly from the aerodynamic model described earlier, rather than being approximated by sine and cosine series of thrust and tip speed as done in (Ref. Roos, 1996). The downward velocity at the far-field is determined by $v_{\text{d},\infty} = \Gamma_{\max}/(2\pi R(\bar{y}_{\text{cg,adv}} - \bar{y}_{\text{cg,retr}}))$. The distances $\bar{e}_{\text{adv}}$ and $\bar{e}_{\text{retr}}$ are defined as the downstream locations where the vortices are considered fully formed:

$$\begin{aligned}\bar{e}_{\text{adv}} &= \frac{2}{9}\pi^2 R^{1/2}(1-\bar{y}(\Gamma=\Gamma_{\max}))^{3/2}\frac{V}{\kappa_{\text{adv}}}\\ \bar{e}_{\text{retr}} &= \frac{2}{9}\pi^2 R^{1/2}(1+\bar{y}(\Gamma=\Gamma_{\max}))^{3/2}\frac{V}{\kappa_{\text{retr}}},\end{aligned} \tag{11}$$

The equations above describe the lateral and axial positions of the disc edge vortices. The cross-sectional shape of these edge vortices, specifically, the spiral that represents the geometry of a disc edge vortex in cross section, is given by Kaden (see Fig.2a):

$$\text{r} = \left(\frac{3}{2}\right)^{1/3}\left(\frac{\kappa t}{\pi\varphi}\right)^{2/3}, \tag{12}$$

where r and φ denote the polar coordinates in a coordinate system whose origin is placed at the center of a disc edge vortex. The corresponding Cartesian coordinates y and z of the cross-section are given by the following expressions:

$$\begin{aligned}\bar{y}_{\text{w,adv}} &= \bar{y}_{\text{c,adv}} - \bar{\text{r}}_{\text{adv}}\cos\varphi, \quad \bar{z}_{\text{w,adv}} = \bar{z}_{\text{c,adv}} - \bar{\text{r}}_{\text{adv}}\sin\varphi,\\ \bar{y}_{\text{w,retr}} &= \bar{y}_{\text{c,retr}} - \bar{\text{r}}_{\text{retr}}\cos\varphi, \quad \bar{z}_{\text{w,retr}} = \bar{z}_{\text{c,retr}} - \bar{\text{r}}_{\text{retr}}\sin\varphi,\end{aligned} \tag{13}$$

where $\bar{\text{r}} = \text{r}/R$, where r is defined in Eq.12.

The prescribed wake model

The prescribed wake geometry consists of a single tip vortex trailing from each blade. The geometry of a skewed, undisturbed helical wake, commonly referred to as a rigid wake, in rotor coordinates can be described based on the operating conditions and momentum theory considerations:

$$\begin{aligned}\bar{x} &= \mu_\infty\psi_w + r_v\cos(\Delta\psi),\\ \bar{y} &= r_v\sin(\Delta\psi),\\ \bar{z} &= -\lambda_i\psi_w,\end{aligned} \tag{14}$$

where $\Delta\psi = \psi_b - \psi_w$, r_v is the normalized radial release point of the trailed vortex filament, which is set to 1 in this study; μ_∞ denotes the advance ratio; ψ_b represents the blade azimuth angle; ψ_w is the wake age; and λ_i is the induced inflow ratio defined as $\lambda_i = v_i/\Omega R$.

Beddoes extended the rigid helical wake model by incorporating vertical displacement of the tip-vortex trajectories (Ref. Beddoes, 1985). This is achieved by modifying the vertical component, $\bar{z}$, of the rigid wake geometry described in Eq. 15. Specifically, in Beddoes' formulation, the vertical coordinate is expressed as $\bar{z} = -\lambda_i \psi_w - \int_0^{\psi_w} \lambda_i \mathrm{d}\psi$. The second term distinguishes Beddoes' contribution. This integral term varies depending on the wake's position relative to the edges of the rotor disk, as detailed below:

$$
\begin{aligned}
&-\lambda_0 \left(1 + E\left(\cos(\Delta\psi) + 0.5\mu\psi_w - |\bar{y}^3|\right)\right)\psi_w, \text{if } \bar{x} < -\cos(\Delta\psi) \\
&-2\lambda_0(1 - E|\bar{y}^3|)\psi_w, \text{ if } \cos(\Delta\psi) > 0 \\
&-\frac{2\lambda_0\bar{x}}{\mu_\infty}(1 - E|\bar{y}^3|), \text{ else} \qquad (15)
\end{aligned}
$$

where λ_0 denotes the mean induced velocity ratio on the rotor disk as predicted by momentum theory, and E represents the vertical displacement envelope function characterizing the wake geometry. Following Beddoes, E is often taken equal to the wake skew angle χ, where χ is defined by the ratio of advance velocity to induced velocity in the rotor inflow. However, Leishman (Ref. Leishman, 2006) suggests that using $E = \chi/2$ typically yields better agreement with experimental measurements, though this parameter should be tuned for each specific rotor configuration when accuracy is paramount. In this study, E is set to $E = 2\pi\lambda_a$, where λ_a denotes the average induced velocity ratio over the rotor disk. This choice is a modeling assumption intended to capture the vertical wake displacement based on induced velocity magnitude; however, its applicability may be limited and should be validated for each case.

GEOMETRY AND NUMERICAL SETUP

The geometry used in this study is a two-bladed propeller designed at TUDelft, and characterized by a radius R = 0.15 m and NACA 4412 airfoil sections. Additional details about the employed geometry can be found in (Ref. Casalino et al., 2021). This propeller has been extensively examined in previous experimental works (Refs. Grande et al., 2022b, Grande et al., 2022a). In the present work, high-fidelity (H-F) CFD simulations, using the commercial software SIMULIA PowerFLOW based on the Lattice-Boltzmann/Very Large Eddy Simulation (LB/VLES) method, have been carried out to generate reference data for validating the analytical model. The computational setup has been successfully validated in the past on the same propeller geometry in several numerical studies (Refs. Romani et al., 2022, Casalino et al., 2022, Casalino et al., 2023), where the interested reader can also find additional information about the LB/VLES flow solver. In the current work, an isolated propeller configuration operated at 4000 RPM under edgewise flow conditions is considered, with a flow incidence angle $\alpha_d = 5°$ and a free-stream velocity $V = 10$ m/s, as sketched in Fig. 3.

The computational domain is a spherical volume of radius 120R centered around the propeller hub at (0, 0, 0) m. Free-stream static pressure (101325 Pa) and velocity (10 m/s), and turbulence intensity of 0.1% of the free-stream velocity are prescribed on its outer boundary. Figure 4 shows the details of the computational grid and setup. The propeller and hub are encompassed by a volume of revolution that defines the

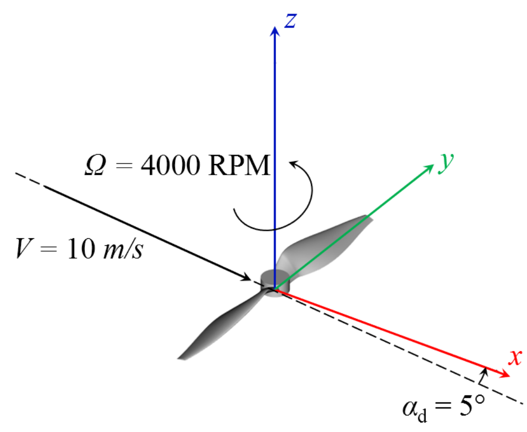

Figure 3: Propeller configuration and operating conditions.

Local Reference Frame (LRF), i.e. the rotating sliding mesh domain used to reproduce the propeller rotation.

The LB/VLES scheme is solved on a Cartesian mesh composed of cubic volume elements (voxels) distributed within different Variable Resolution (VR) regions. A grid resolution change by a factor of two characterizes adjacent VRs. A total of 14 VR regions are used to discretize the whole fluid domain, with the finest resolution level (VR13) placed around the blade. A resolution of 100 voxels along the mean chord (22.85 mm) is used within this finest resolution level, resulting in a smallest voxel size of 0.022 mm, a mean $y^+ \simeq 5$ on the blade surface. The second finest VR is applied on the whole propeller geometry and in the near tip vortex region, while the third finest level (VR11) is used to finely discretize the propeller wake region, thus allowing the comparison with the analytical models for a sufficient number of wake spirals. All the other VRs consist of boxes or spheres that are used to discretize the rest of the fluid domain up to its boundaries. The overall mesh consists of 188 million voxels and 41.4 million fine-equivalent voxels. The whole fluid domain is initialized with the instantaneous flow solution from a statistically converged coarser simulation. Hence, after a settling time corresponding to 2 propeller revolutions, the sampling of relevant flow data is started for 2 additional revolutions.

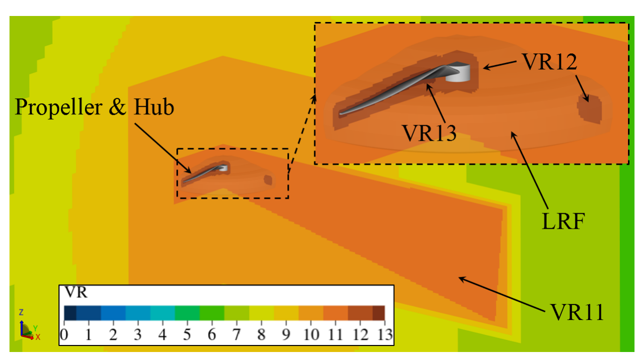

Figure 4: Details of the computational setup and grid.

VALIDATION RESULTS

The computational accuracy of the aerodynamic model is validated by comparing the prediction of loading distributions over the rotor disk against the high-fidelity (H-F) simulation results.

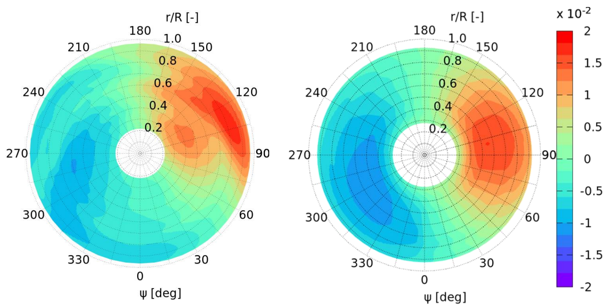

(a) H-F CFD simulation (left), Peters-He model (right).

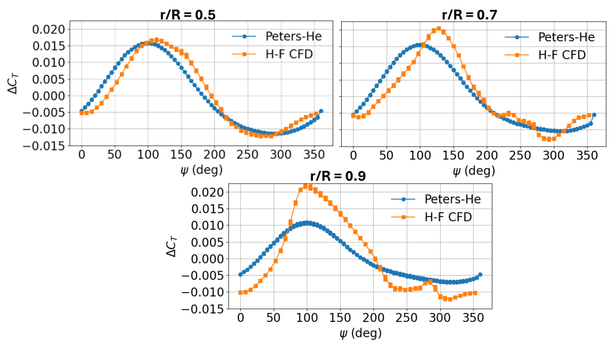

(b) ΔC_T at three radial stations.

Figure 5: Comparison of fluctuating thrust coefficient $\Delta C_{\partial rT}$ over the rotor disk (a) and at three radial stations r/R=0.5, r/R=0.7 and r/R=0.9.

The fluctuating, mean-removed sectional thrust distribution, $\Delta C_{\partial rT}$, is compared in Fig. 5. As seen from $\Delta C_{\partial rT}$ distribution over rotor disk as shown in Fig. 5a, the implementation of the Peters-He model in LOPNOR-ARDYN captures the general trend of the thrust distribution over the rotor disk well, except for an underprediction in the region between 90° and 120° and slight overprediction in the region between 240° and 270°. This discrepancy may be attributed to the chosen number of harmonics and polynomial terms, m and n, respectively, which could be adjusted to improve the agreement. However, a large improvement is not expected as increasing m and n only yields incremental improvements as verified by (Ref. Ho and Yeo, 2021). To further evaluate the agreement between the Peters–He model and H-F CFD data, $\Delta C_{\partial rT}$ is compared at three radial positions. As shown in Fig.5b, good agreement is observed at $r/R = 0.5$ and $r/R = 0.7$, while a considerable underprediction appears near the edges of the rotor disk. The cause of this discrepancy is still under investigation and will be addressed in future work. Overall, the results demonstrate favorable agreement between the high-fidelity CFD simulation and the aerodynamic model used to generate input data for the prediction of wake trajectories.

Since the disk edge vortex model employed in this study is based on time-averaged assumptions, the time-averaged CFD data is used to validate the analytical wake model. In contrast, the phase-locked averaged CFD data is used to validate the Beddoes prescribed wake model. Figure 6 illustrates the iso-surfaces of λ_2 (with a value of -75000 s^{-2}), colored according to the vorticity magnitude, which ranges from 0 to 1500 s^{-1}.

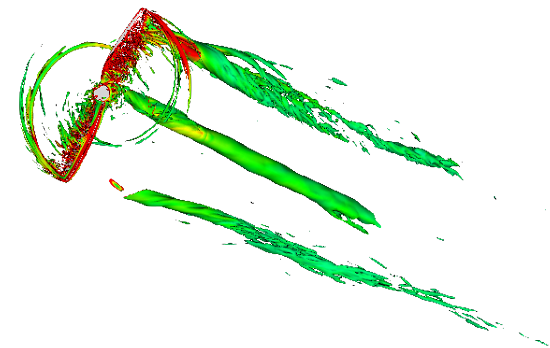

(a) Time averaged.

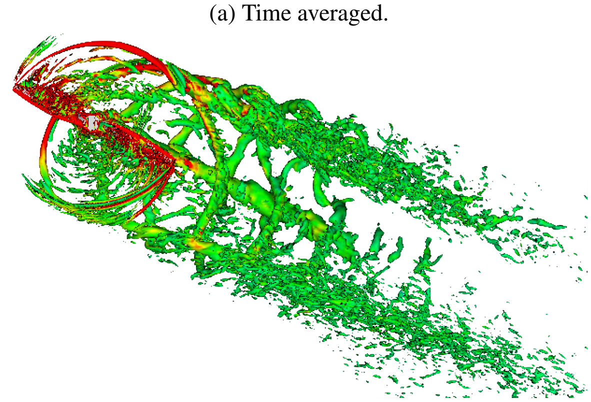

(b) Phase-locked averaged.

Figure 6: Iso-surface of λ_2 (value -75000) of time averaged (a) and phase-locked averaged (b) vortical structures.

To validate the lateral and axial positions of the disk edge vortices, the time-averaged vortical structures obtained from H-F CFD simulations (Fig.6a) are extracted and visualized alongside the predicted disc edge vortex trajectories in Fig.7. The analytical model shows good agreement with the CFD data in predicting both the lateral and axial positions of the disk edge vortices on both the advancing and retreating sides of the rotor. In particular, the lateral positions of the edge vortices are well captured by the analytical model when compared with the high-fidelity CFD results. Regarding the axial positions, as shown in Fig.7b, the wakes on the advancing side are deflected more downward due to the higher lift generated in this region. In contrast, the edge vortices on the retreating side remain nearly level with the rotor disk and deflect downward more gradually. This behavior is primarily attributed to significant flow separation on the retreating side, as also observed in Fig.6. The reduced lift in this region results in weaker circulation along the edge vortices, leading to smaller downward deflection compared to the advancing side. Similar trends have been reported in (Ref. Misiorowski et al., 2019). Overall, the analytical model demonstrates good agreement with the high-fidelity CFD data and confirms its reliability in predicting the edge vortex trajectories.

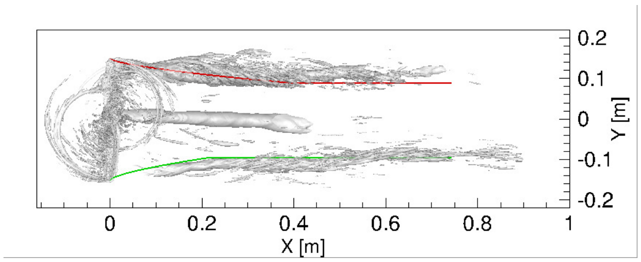

(a) Disc edge vortices lateral location.

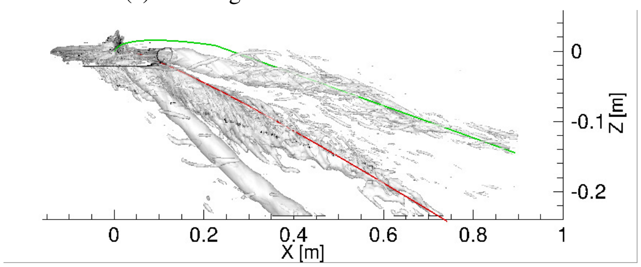

(b) Disc edge vortices axial location.

Figure 7: Comparison of lateral and axial locations of edge vortices calculated with analytical model against H-F simulation data.

The tip vortex geometries predicted by the Beddoes prescribed wake model are compared with phase-locked averaged high-fidelity (H-F) CFD simulation results, as shown in Fig. 8. The prescribed model captures the overall trend in the lateral positions of the tip vortices reasonably well. However, it fails to predict the rolled-up tip vortex structures observed in the region enclosed by X=[0.35,0.45] and Y=[0,0.1] on the advancing side (positive Y-axis), due to an inherent limitation of the Beddoes model—namely, its reliance on undistorted helical trajectories for the vortex filaments. Despite this, the model accurately predicts the axial positions of the tip vortices shed by both blades. Overall, the Beddoes prescribed wake model shows good agreement with the H-F CFD results, particularly in predicting the axial locations of the tip vortices, thereby confirming its reliability for estimating their spatial distribution.

Fig. 9 compares the cross-sectional geometry of the rolled-up disc-edge vortices on both the advancing and retreating sides of the rotor, at three vertical stations downstream of the rotor disk. The analytical solution captures the general trends in the vortex cross-sections on both sides. On the advancing side, the analytical predictions show very good agreement with the high-fidelity (H-F) CFD data at all three stations. On the retreating side, the agreement improves with increasing downstream distance from the rotor disk.

CONCLUSION

This work presents a computational approach that combines an aerodynamic model based on the Peters–He finite-state dynamic inflow model with an analytical wake model for predicting the disc edge vortex and a prescribed wake model for predicting trailed tip vortices. High-fidelity CFD simulations using the commercial software SIMULIA PowerFLOW are carried out to validate the proposed approach. Both time-averaged and phase-locked averaged CFD data are used to validate the analytical and prescribed wake models, respectively.

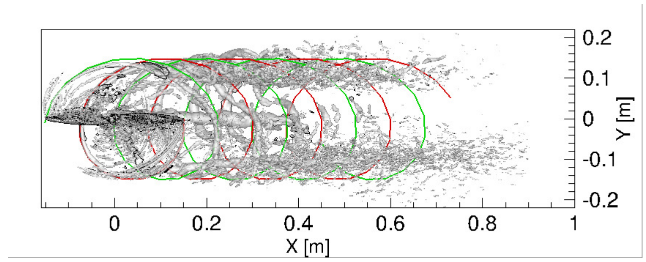

(a) Tip vortices lateral location.

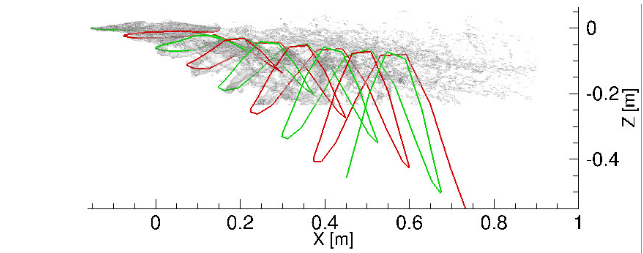

(b) Tip vortices axial location.

Figure 8: Comparison of tip vortex trajectories calculated with the Beddoes prescribed wake model against phase-locked averaged H-F CFD simulation data.

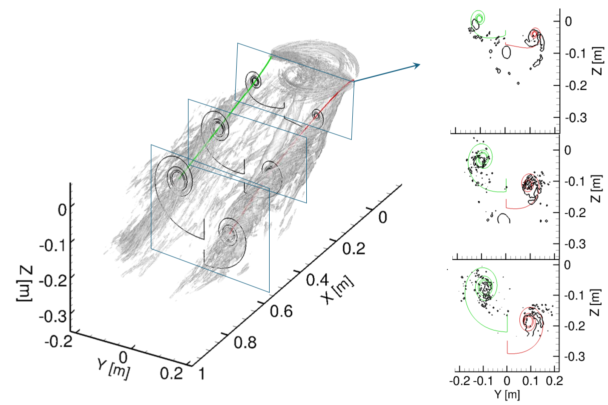

Figure 9: Comparison of analytical predictions with H-F CFD flow data at three vertical stations along downstream direction.

The results show good agreement with the CFD data, demonstrating accurate predictions of aerodynamic loading on the rotor disk as well as the lateral and axial positions of the edge vortex and trailed tip vortices from each blade. This approach offers a valuable tool for future applications involving blade–wake interactions, blade–vortex interaction noise prediction, and noise-optimal trajectory optimization in eVTOL operations for future air mobility.

REFERENCES

Beddoes, 1985. Beddoes, T. (1985). A wake model for high resolution airloads. In *International Conference on Rotorcraft Basic Research*.

Casalino et al., 2021. Casalino, D., Grande, E., Romani, G., Ragni, D., and Avallone, F. (2021). Definition of a benchmark for low reynolds number propeller aeroacoustics. *Aerospace Science and Technology*, 113:106707.

Casalino et al., 2023. Casalino, D., Romani, G., Pii, L. M., and Colombo, R. (2023). Flow confinement effects on sUAS rotor noise. *Aerospace Science and Technology*, 143:108756.

Casalino et al., 2022. Casalino, D., Romani, G., Zhang, R., and Chen, H. (2022). Lattice-Boltzmann calculations of rotor aeroacoustics in transitional boundary layer regime. *Aerospace Science and Technology*, 130:107953.

Grande et al., 2022a. Grande, E., Ragni, D., Avallone, F., and Casalino, D. (2022a). Laminar separation bubble noise on a propeller operating at low Reynolds numbers. *AIAA Journal*, 60(9):5324–5335.

Grande et al., 2022b. Grande, E., Romani, G., Ragni, D., Avallone, F., and Casalino, D. (2022b). Aeroacoustic investigation of a propeller operating at low Reynolds numbers. *AIAA Journal*, 60(2):860–871.

Ho and Yeo, 2021. Ho, J. C. and Yeo, H. (2021). Evaluation of finite-state dynamic inflow for rotors. *Journal of Aircraft*, 58(5):1068–1082.

Kaden, 1931. Kaden, H. (1931). Aufwicklung einer unstabilen unstetigkeitsfläche. *Ingenieur-Archiv*, 2(2):140–168.

Kinner, 1937. Kinner, W. (1937). *The Principle of the Potential Theory Applied to the Circular Wing*. Springer.

Komerath et al., 2011. Komerath, N. M., Smith, M. J., and Tung, C. (2011). A review of rotor wake physics and modeling. *Journal of the American Helicopter Society*, 56(2):22006–22006.

Leishman, 2006. Leishman, G. J. (2006). *Principles of helicopter aerodynamics with CD extra*. Cambridge university press.

Li, 2020. Li, S. (2020). *Development of Rotorcraft Forward Flight Analysis Code Using the Finite-State Dynamic Inflow Model*. PhD thesis, Master's thesis, University of California Davis.

Luo et al., 2015. Luo, J., Zhu, L., and Yan, G. (2015). Novel quadrotor forward-flight model based on wake interference. *AIAA Journal*, 53(12):3522–3533.

Misiorowski et al., 2019. Misiorowski, M., Gandhi, F., and Oberai, A. A. (2019). Computational study on rotor interactional effects for a quadcopter in edgewise flight. *AIAA Journal*, 57(12):5309–5319.

Moriarty and Hansen, 2005. Moriarty, P. J. and Hansen, A. C. (2005). Aerodyn theory manual. Technical report, National Renewable Energy Lab., Golden, CO (US).

Peters and He, 1995. Peters, D. A. and He, C. J. (1995). Finite state induced flow models. ii-three-dimensional rotor disk. *Journal of Aircraft*, 32(2):323–333.

Romani et al., 2022. Romani, G., Grande, E., Avallone, F., Ragni, D., and Casalino, D. (2022). Computational study of flow incidence effects on the aeroacoustics of low blade-tip mach number propellers. *Aerospace Science and Technology*, 120:107275.

Roos, 1996. Roos, J. (1996). An analytical model for the determination of disc edge vortex strength, location and geometry at low to intermediate flying speeds. In *22nd European Rotorcraft Forum, Brighton (U.K.)*.

Spreiter and Sacks, 1951. Spreiter, J. R. and Sacks, A. H. (1951). The rolling up of the trailing vortex sheet and its effect on the downwash behind wings. *Journal of the Aeronautical Sciences*, 18(1):21–32.

Usov et al., 2022. Usov, D., Appleton, W., Filippone, A., and Bojdo, N. (2022). Low-order aerodynamic model for interference in multirotor systems. *Journal of Aircraft*, 59(6):1450–1462.

Wang et al., 2021. Wang, C., Huang, M. Q., Ma, S., Wang, H. W., and Tang, M. (2021). Main rotor wake interference effects on tail rotor thrust in crosswind. *International Journal of Aerospace Engineering*, 2021(1):9994115.

Yunus et al., 2025. Yunus, F., Pavel, M. D., Romani, G., Sinnige, T., Casalino, D., and Snellen, M. (2025). Efficient prediction of aerodynamic interference in multirotor systems during forward flight. In *51th European Rotorcraft Forum, Venice (Italy)*.